catalysts

MDPI

*Article*

# Pyrite Cinder as an Effective Fenton-like Catalyst for the Degradation of Reactive Azo Dye: Effects of Process Parameters and Complete Effluent Characterization

**Djurdja Kerkez [1,*], Milena Bečelić-Tomin [1], Vesna Gvoić [2], Aleksandra Kulić Mandić [1], Anita Leovac Maćerak [1], Dragana Tomašević Pilipović [1] and Vesna Pešić [1]**

[1] Department of Chemistry, Biochemistry and Environmental Protection, Faculty of Sciences, University of Novi Sad, Trg Dositeja Obradovića 3, 21000 Novi Sad, Serbia
[2] Department of Graphic Engineering and Design, Faculty of Technical Sciences, University of Novi Sad, Trg Dositeja Obradovića 6, 21000 Novi Sad, Serbia
* Correspondence: djurdja.kerkez@dh.uns.ac.rs; Tel.: +381-21-4852734

**Abstract:** This research investigates the potential use of pyrite cinder (PC) as an efficient Fenton-like catalyst for the removal of the reactive azo dye Reactive Red 120 (RR120) from aqueous solutions. The characterization of its PC structure and composition confirmed its great potential to act as catalytic iron source in a heterogeneous Fenton system. Dye removal optimization was performed in terms of PC dosage (0.4–8 g/L), $H_2O_2$ concentration (2–25 mM), pH value (2–4.6), initial dye concentration (50–200 mg/L), and mixing time. The highest decolorization efficiency (92%) was achieved after a reaction time of 480 min under following conditions: RR120 = 50 mg/L, PC = 4 g/L, $H_2O_2$ = 10 mM, and pH = 3. After decolorization, an extensive analysis of the generated effluent was performed regarding metal leaching, mineralization, toxicity, and degradation product formation. The metal leaching indicated the necessity for a pH increase in order to remove the settled metal hydroxides. The mineralization efficiency was satisfactory, reaching 85% and 62% of the COD and TOC removal, respectively. The respirometry measurements and bioluminescence tests indicated the detoxification of the treated solution. The absorption spectra and GC/MS analysis confirmed the changes in the molecular structure in the form of the destruction of the azo bond, with a simpler aromatic and aliphatic intermediates formation. This study provides an effective method for removing azo dye in polluted water by employing waste tailings as alternative Fenton-like catalysts, while also using waste tailings as the secondary resource.

**Keywords:** industrial waste valorization; pyrite cinder; heterogeneous Fenton-like process; decolorization



**Citation:** Kerkez, D.; Bečelić-Tomin, M.; Gvoić, V.; Mandić, A.K.; Leovac Maćerak, A.; Tomašević Pilipović, D.; Pešić, V. Pyrite Cinder as an Effective Fenton-like Catalyst for the Degradation of Reactive Azo Dye: Effects of Process Parameters and Complete Effluent Characterization. *Catalysts* **2023**, *13*, 424. https://doi.org/10.3390/catal13020424

Academic Editor: Maria Cornelia Iliuta

Received: 28 December 2022
Revised: 8 February 2023
Accepted: 13 February 2023
Published: 16 February 2023



## 1. Introduction

Environmental remediation processes cover a wide range of studies based on mineral material applicability. One such process is wastewater treatment which, when conducted with the use of mineral materials, has a low cost and optimal environmental harmony, in comparison when using synthetic compounds [1–3]. Pyrite ($FeS_2$) is an iron sulphide mineral that is available in large quantities in the earth's crust [4]. It is widely applied in sulphuric acid production by roasting its concentrates, during which an iron-rich waste product is left as a residue [5–7]. In theory, approximately 67% of pyrite in the feed is converted to pyrite cinder (PC) during this process. The stockpiles of this type of waste occupy a large area of land and can easily be affected by aeolian erosion and topple, having as a consequence vegetation deterioration and environmental pollution. Alternatively, PC can represent an alternative source of iron since it is composed mainly of iron oxides. Considering the fact that this type of waste is enriched with iron oxides, the possibility of

its implementation as a catalytic iron source in heterogeneous Fenton-like processes when treating wastewater should be investigated.

Due to the high quantities of water used in dyeing processes, textile manufacturing is responsible for the production of large wastewater volumes which are characterized by high-intensity color, high chemical oxygen demand (COD), highly fluctuating pH, and biotoxicity [8,9]. Untreated effluents from these industries cause water bodies to become colored, and they interfere with the natural growth activity of aquatic life by blocking sunlight and stopping the re-oxygenation capacity of water [10,11]. Under the distinctive aerobic conditions taking place in conventional biological treatment systems, reactive dyes are known as non-degradable materials which adsorb at very low levels on biological solids, having residual color in discharged effluents as a result [12,13]. Up to 70% of the dyes currently available on the market are azo compounds that are recalcitrant to conventional biological and physicochemical treatments [14]. In addition to color-related issues they can cause, the environmental impacts of these dyes are also reflected by the numerous azo dyes and their breakdown products (which are frequently colorless amines) toxicity and/or mutagenicity to living organisms [9]. The conventional strategies for the purification of dyeing wastewater, such as coagulation and flocculation and adsorption and ultrafiltration, were investigated to remove the azo dyes from the wastewater [15,16]. However, these processes do not destroy dye molecules; rather, they transfer them from one phase to another [17]. Another extensively used way to treat dye wastewaters is biological treatment. The main disadvantage of this method is its long treatment period with quite limited success as it is not able to achieve "destructive" decolorization since the textile dyes are deliberately designed to resist biological, photolytic, and chemical degradation [18,19]. All these processes can be expensive and inefficient, and they frequently produce large amounts of secondary waste [20].

Advanced oxidation processes (AOPs), on the other hand, are considered promising technologies involving the in situ production of strong oxidants, primarily hydridooxygen and hydridodioxygen radicals ($HO^{\bullet}$ and $HO_2^{\bullet}$, respectively), which are able to rapidly and non-selectively oxidize a wide range of refractory pollutants [20–25]. Advanced oxidation processes are a group of wastewater treatment techniques characterized as destructive, with high oxidation efficacy and an absence of secondary pollution formation. Advanced oxidation processes can be performed through various methods such as ozonization, electrochemical treatment, the Fenton process, photolysis, sonolysis, etc. The main advantages (A) and disadvantages (D) of most of the applied advanced oxidation methods can be summarized as follows: ozone oxidation: A—higher oxidation potential compared to chlorine, powerful oxidizer, inhibits both bacteria and fungus, and renewable source, and D—high concentration dosage required, expensive, and complex process; electrochemical oxidation: A—removes highly toxic compounds, no hazardous by-products, novel contaminants treated, and no additional catalyst is needed, and D—energy source needed, electrode maintenance, and time consuming; Fenton process: A—high organic removal, high performance, $H_2O_2$ breaks easily, and operated at room temperature and pressure, and D—more ferrous sludge produced, complex pH, and risks with storage and handling reagents; photolysis and photocatalysis: A—uses natural energy sources, low catalyst used, minimal cost, and high physical stability, and D—low pH needed, difficulty in isolation of catalyst, and poor selective adsorption; sonolysis: A—no chemicals used, medical drugs removed, and short time reaction, and D—machines undergo wear and tear, low efficiency, and high cost. A critical approach and a full evaluation are given in detail in the study by Saravanan et al., 2022 [26–30].

Among these advanced oxidation methods, the use of Fenton's reagent has proven to be an attractive treatment method. It is simple and low-cost process, taking place under mild operating conditions. The homogeneous Fenton and Fenton-like processes involve the reaction of hydrogen peroxide with ferrous ($Fe^{2+}$) and ferric ($Fe^{3+}$) ions to produce hydroxyl radicals. However, the classic homogeneous Fenton reaction has some critical downsides, such as the formation of ferric hydroxide sludge, which requires further separation and

causes the early termination of the reaction. To overcome these disadvantages, various heterogeneous Fenton-like catalysts have recently been developed as a more practical and efficient alternative technique [31,32]. Heterogeneous Fenton oxidation typically requires robust catalysts for practical applications. Great efforts have been made to design and produce novel heterogeneous Fenton catalysts, including various iron oxides and zero-valent irons and a novel class of iron-based metal-organic frameworks (Fe-MOFs) [33,34]. Iron and other transition metals, such as cobalt, have been proven to effectively initiate reactive species generation under mild conditions or to activate different agents to produce various active species [35–38].

Numerous studies have suggested that a surface-catalyzed process in the heterogeneous reaction using iron oxides (e.g., magnetite, goethite, and hematite) can control the decomposition of $H_2O_2$. The interactions between oxidant and iron surface sites (≡Fe) are explained by heterogeneous reactions analogous to the solution phase reactions, where the dominant reaction is first in a chain of reactions occurring on the mineral surface (as set out in Equations (1)–(10)) [39]:

$$\equiv Fe^{2+} + H_2O_2 + H^+ \rightarrow \equiv Fe^{3+} + HO^{\bullet} + H_2O \quad (1)$$

$$\equiv Fe^{2+} + H_2O_2 \rightarrow \equiv Fe^{3+} + HO^- + HO\bullet \quad (2)$$

$$\equiv Fe^{3+} + H_2O_2 \rightarrow \equiv Fe^{3+}(H_2O_2) \quad (3)$$

$$\equiv Fe^{3+}(H_2O_2) \rightarrow (\equiv Fe^{2+}\bullet O_2H) + H^+ \quad (4)$$

$$(\equiv Fe^{2+}\bullet O_2H) \rightarrow \equiv Fe^{2+} + HO_2\bullet/O_2\bullet^- \quad (5)$$

$$\equiv Fe^{3+} + O_2\bullet^- \rightarrow \equiv Fe^{2+} + O_2 \quad (6)$$

$$\equiv Fe^{2+} + HO_2\bullet/O_2\bullet^- \rightarrow \equiv Fe^{3+} + HO^{2-} \quad (7)$$

$$\equiv Fe + RR120 \leftrightarrow \equiv Fe(RR120)s \quad (8)$$

$$\equiv Fe(RR120)s + HO\bullet \rightarrow \equiv Fe + (RR120\ by\text{-}products)_{solution} \rightarrow CO_2 + H_2O \quad (9)$$

$$HO\bullet + RR120_{solution} \rightarrow (RR120\ by\text{-}products)_{solution} \rightarrow CO_2 + H_2O \quad (10)$$

Different kinds of iron-bearing materials have been closely studied for Fenton-like reactions, among which iron minerals, such as pyrite, goethite, and ferrihydrite have attracted more attention because of their abundance, stability, lower slurry formation, lower costs, and possible effortless separation and recycling [40–42]. The interest in possible alternative uses of solid wastes as adsorbents and catalysts, or as the starting materials before their discharge into the environment, is increasing.

The present study focused on the following objectives: (1) PC characterization as a possible catalyst in Fenton-like systems, (2) establishing the optimum operating conditions to achieve the highest decolorization efficiency of the reactive azo dye Reactive Red 120 (RR120) in aqueous solutions using PC/$H_2O_2$ in a modified heterogeneous Fenton process; (3) characterization of the generated effluent with respect to leached metals and arsenic from PC; (4) determination of the mineralization efficiency as an indication of the persistent dye molecules degradation; and (5) identification of the nature of the degradation products in the treated effluent, as well as the determination of the biodegradability and toxicity of the obtained effluent.

## 2. Results and Discussion

The SEM image (Figure 1a) indicated that the PC sample represented non-uniformly shaped particles with rough and granular textures and large amounts of open porosity. Regarding their size, the particles differed, ranging from 0.1–2.5 μm, similar to natural pyrite [4]. The energy dispersive X-ray spectrum of the elements confirmed the presence of Fe and O (Figure 1b,c). These characteristics may have influenced the availability of the superficial iron for the catalysis of the heterogeneous Fenton process [43]. The XRD

patterns proved that the primary diffraction peaks belonged to hematite, magnetite, and quartz (Figure 1d).

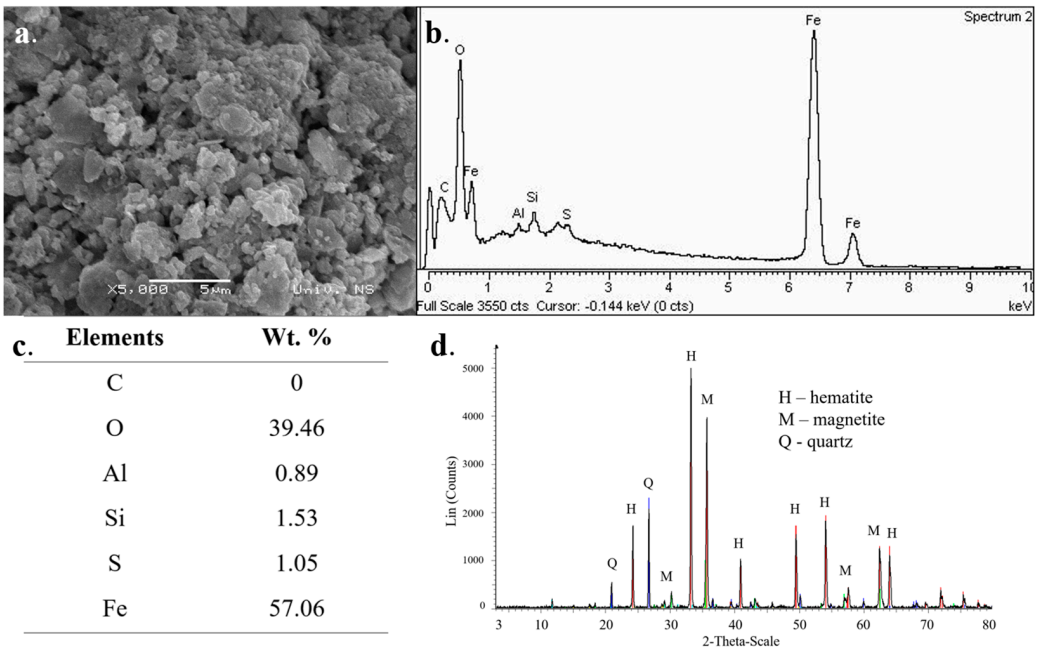


| Elements | Wt. % |
|---|---|
| C | 0 |
| O | 39.46 |
| Al | 0.89 |
| Si | 1.53 |
| S | 1.05 |
| Fe | 57.06 |

**Figure 1.** (**a**) SEM image of the PC sample. (**b**) The corresponding element analysis by EDX. (**c**) EDX results table. (**d**) X-ray diffraction profile of the PC sample.

The XRD-XRF analysis (Table 1) provided the chemical composition of pyrite cinder sample, confirming that it largely consisted of hematite, together with magnetite, and a considerable proportion of quartz. In addition, some secondary minerals belonging to a group of carbonates (calcite), oxides (rutil and periclase), silicates (mullite, alite, plagioclase, gehlenite, cristobalite, and K feldspar), sulphates (thenardite), and some amorph fly ash were detected in small quantities. These findings are in good correlation with previous studies of pyrite cinder composition (though they were intended for different purposes) [44]. Large amounts of readily available iron oxides were present in the PC, and they were the basis of its further use as a catalyst in the heterogeneous Fenton process.

**Table 1.** Chemical composition of the pyrite cinder.

| Compound | Stoichiometric Forms | Content (%) |
|---|---|---|
| Hematite | $Fe_2O_3$ | 74.6 |
| Quartz | $SiO_2$ | 11.9 |
| Magnetite | $Fe_3O_4$ | 4.69 |
| Mullite | $3Al_2O_3$ $2SiO_2$ or $2Al_2O_3$ $SiO_2$ | 2.30 |
| Alite | Tricalcium silicate ($Ca_3SiO_5$) | 2.21 |
| Plagioclase | Respective compositions of $NaAlSi_3O_8$ and $CaAl_2Si_2O_8$ | 2.018 |
| Rutil | Most common natural form of $TiO_2$ | 0.885 |
| Calcite | $CaCO_3$ | 0.624 |
| Gehlenite | Sorosilicate($Ca_2Al(AlSiO_7)$) | 0.478 |
| Cristobalite | High-temperature polymorph of silica ($SiO_2$) | 0.121 |
| Periclase | Cubic form of magnesium oxide (MgO) | 0.087 |
| Thenardite | Anhydrous sodium sulphate mineral ($Na_2SO_4$) | 0.025 |
| Flyash-amorph | / | 0.009 |
| K-Feldspar | a group of rock-forming tectosilicate minerals ($KAlSi_3O_8$-$NaAlSi_3O_8$-$CaAl_2Si_2O_8$) | 0.005 |

The structural characteristic of PC, derived from the $N_2$ adsorption-desorption isotherms, showed that the BET specific surface area was quite low (3.114 $m^2/g$). Additionally, from

the aspect of the mesopores, the BJH total pore volume was 0.032 $cm^3/g$, with an average pore diameter of ~40 nm, indicating that this material was roughly mesoporous. Mesoporosity is considered one of the most favorable characteristics of efficient heterogeneous Fenton catalysts [41,42,45]. Micropores were not detected in the PC sample.

To understand the properties of the heterogeneous Fenton system with PC usage, the decolorization of RR120 was investigated in different reaction systems (Figure 2).

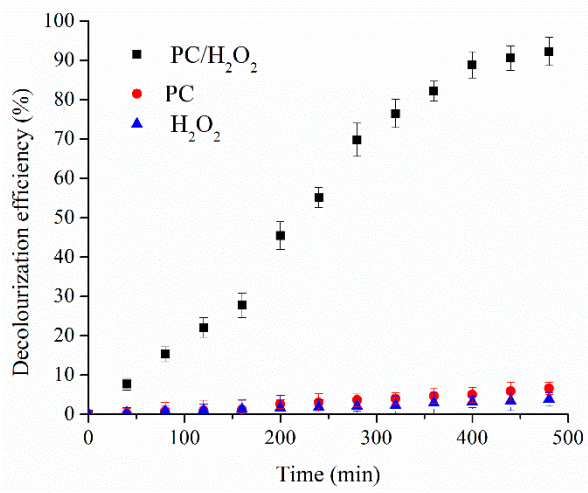


**Figure 2.** Comparison of the RR120 decolorization efficiency in the various processes under the experimental conditions (RR120 = 50 mg/L, PC = 4 g/L, $H_2O_2$ = 10 mM, and pH = 3).

The results showed that there was no obvious oxidation of the dye by the $H_2O_2$ without the PC as the decolorization efficiency after 480 min was 3.8%. The potential losses due to the RR120 molecule adsorption on the PC surface were also negligible (no more than 6.6% after 8 h). Approximately 92.3% of the RR120 was degraded in the PC/$H_2O_2$ within the same time. Thus, the results revealed that the enhanced removal of the RR120 was attributed to the heterogeneous Fenton-like process.

### *2.1. Optimization of Operating Conditions for Dye solution Decolourization*

The influence of the PC concentration on the efficiency of the decolorization of the synthetic aqueous solution of RR120 is shown in Figure 3a. The tested PC concentration was in the range of 0.4–8 g/L. The results implied that the $Fe^{2+}$-generating reactions were a rate-limiting step during the dye oxidation. As the PC dosage increased, the $Fe^{2+}$ concentration also increased due to the Fe (III) reduction, leading to enhanced $HO^{\bullet}$ formation and, therefore, to the RR120 oxidation acceleration [37,46]. Furthermore, the PC increase led to a more accessible surface on which the reaction could occur, which enabled a greater production of $HO^{\bullet}$ radicals, to a certain extent [47]. Further increases in catalyst dosages (more than 4 g/L) did not cause any significant increases in the oxidation rates. High concentrations of iron ions can lead to the scavenger effect, reducing the reactive species ($HO^{\bullet}$) [40,48,49]. The latter probes used the PC concentration of 4 g/L.

Figure 3b represents the decolorization efficiency in relation to the applied initial hydrogen-peroxide concentration (2–25 mM). The highest decolorization efficiency was attained at an initial concentration of 10 mM of $H_2O_2$. With the initial increase in $H_2O_2$ concentration to 10 mM, the increased hydroxyl radicals enhanced the decolorization ability of the system [10]. The effect of the decolorization efficiency reduction at higher $H_2O_2$ concentrations could be interpreted as being due to a phenomenon where molecules of $H_2O_2$ express a "scavenging" effect towards $HO^{\bullet}$, causing the formation of fewer reactive species, such as $HO_2^{\bullet}$, according to Equation 11 [18,50,51].

$$H_2O_2 + HO\bullet \rightarrow H_2O + HO_2\bullet \quad (11)$$

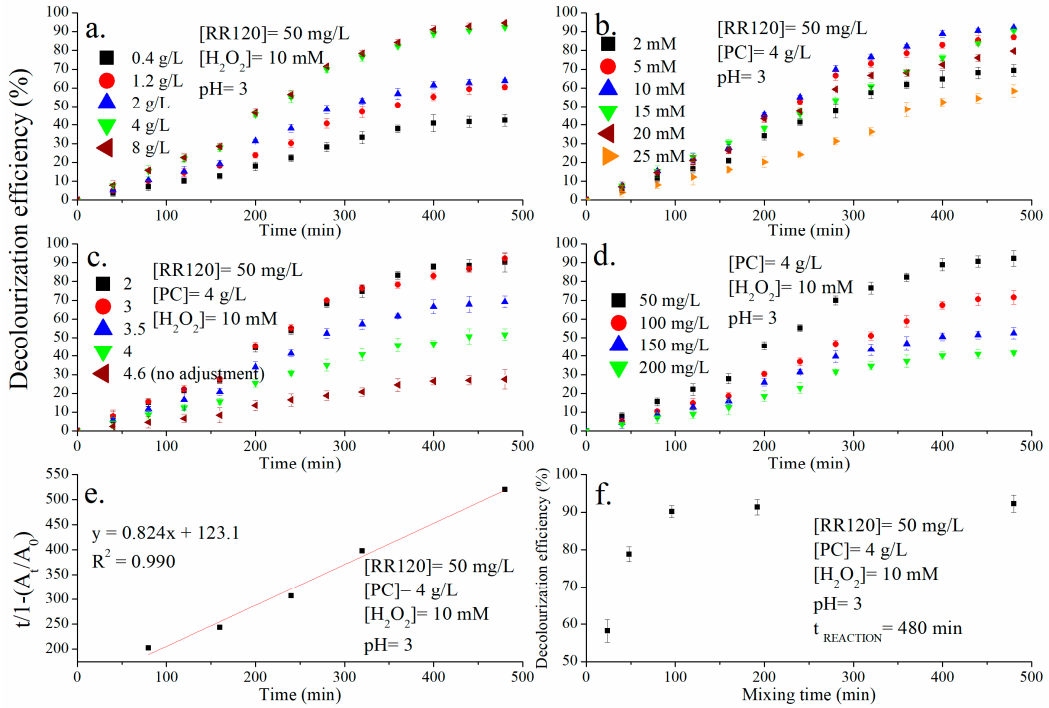


**Figure 3.** Optimization of the RR120 solution decolorization. (**a**) Effect of PC dosage. (**b**) Effect of $H_2O_2$ concentration. (**c**) Effect of initial solution pH. (**d**) Effect of initial dye concentration. (**e**) Kinetics. (**f**) Required mixing time.

Varying pH values can impact heterogeneous Fenton reactions, which take place on the surface of a catalyst [52]. The effect of pH on the decolorization efficiency was examined within the pH values of 2 to 4. In addition, one experiment was performed where the pH of the dye solution was not further adjusted. The results indicated that the Fenton process with the use of PC as a source of iron showed the highest efficiency for a pH of 3 (Figure 3c) [53]. This behavior was observed in similar studies as pH levels near 3 are typically optimum for Fenton and Fenton-like processes. The decolorization efficiency declined with the increasing pH value as the stability of the hydrogen peroxide decreased [21]. The oxidative degradation of the RR120 in the PC Fenton system could be inhibited at high pH values due to the low aqueous Fe(II) concentrations. It has been reported that aqueous Fe(II) leading to the decomposition of $H_2O_2$ to HO• has rarely been detected at pH values higher than 4.5. This suggests that an acidic environment is required for the proper operation of a classic Fenton system to efficiently form HO• by avoiding the precipitation of $Fe(OH)_3$(s). The acidity of the PC itself rapidly decreased the pH of the dye solution. Consequently, there was less acid to be used to adjust the pH value of the solutions, which may be an additional economic advantage of using PC in this type of process.

The influence of the initial dye concentration on the decolorization efficiency is presented in Figure 3d. It can be seen that the oxidation ability of this AOP process was greatly affected by the initial dye load. The negative effect on decolorization at higher RR120 concentrations can be elcudiated by the decrease in the molar ratio of the oxidant/dye molecule. As the initial dye concentration increased, the amount of hydrogen peroxide molecules initially present in the reaction mixture stayed the same, as did the amount of HO• radicals present, which caused this effect [21]. Hence, the generated HO• radicals were too limited to attack the RR120 molecules under these experimental conditions. Additionally, heterogeneous Fenton reactions are partially executed on a catalyst's surface. Consequently, at high dye concentrations, the competitive adsorption of dye molecules will take place, reducing the number of active sites [54].

For the analysis of the decolorization kinetic and to fully utilize the results in real applications, a mathematical model, shown as Equation 13, was used to represent the linear model of the reaction kinetics model. This model generally describes the reaction kinetics, and it was chosen because the whole process cannot describe the kinetics of simple reactions. Regarding the kinetics analysis, the results of the regression with a high value of $R^2$ (0.990) confirmed the possibility of using the chosen model to analyze the decolorization efficiency kinetics (Figure 3e). The chosen model allows for obtaining two characteristic constants (b and m) that are related to the reaction kinetics and the oxidation capacity. The obtained constants and their reciprocal values were as follows: b—0.824; 1/b—1.21; m—123.1; and 1/m—0.0081. Higher 1/m values indicated fast initial decay rates of the RR120. Furthermore, when the reaction time increased, the reciprocal value of constant b increased, reaching the theoretical maximum of dye removal. To fully quantify these two constants, m and b are correlated with iron/hydrogen peroxide ratios, and the reciprocal values for both constants are inversely proportional to those ratios (the lower the values of 1/b and 1/m, the higher the ratio needed). Relatively low 1/b and 1/m values of the derived coefficients indicated that using PC as an iron source in heterogeneous Fenton systems required longer periods of time for achieving effective decolorization when compared to a homogeneous Fenton system, and that higher iron/hydrogen peroxide ratios are needed [55,56]. In PC, Fe(III) is the main iron species, and the reaction rate of Fe(III)/$H_2O_2$ is much slower than that of Fe(II)/$H_2O_2$. In addition, a limited mass transfer in a heterogeneous system results in the lower reactivity of the $H_2O_2$ decomposition [41].

PC, being a material of a high density, tends to settle right after the mixing of the reaction solution is stopped. The required mixing time was investigated to examine whether there was a need for the constant mixing of the solution bulk and to elucidate the primary mechanism responsible for the dye oxidation. In the series of experiments, mixing of the solutions was stopped at 24, 48, 96, 192, and 480 min (constant mixing). Final absorbance was measured at the same time (after 480 min). Investigation of the mixing time effect indicated that there was no need for a constant mixing of the dye solution in order to achieve a high decolorization efficiency. A mixing period of ~90 min was satisfactory for further decolorization. This indicated that in the beginning of the process, catalyzed RR120 oxidation was carried out on the PC surface, as well as in the homogeneous solution. After the cessation of the required stirring, the solution $HO^{\bullet}$ was largely produced from the dissolved iron, and the Fenton reactions were also carried out through reaction intermediates. Overall, the catalytic activity of PC was a combination of the activity of the solid catalysts and the activity of the dissolved, leached iron, as previously investigated by Becelic-Tomin et al. [5]. This is of particular importance from an economic aspect because in spite of the longer duration of the process, a satisfying decolorization efficiency can be achieved within a relatively short mixing time, which reduces the requirements for power consumption (Figure 3f).

The optimal experimental conditions established were: RR120 = 50 mg/L, PC = 4 g/L, $H_2O_2$ = 10 mM, and pH = 3, and so the further characterization was performed on this effluent after 480 min of reaction.

### *2.2. Effluent Characterization*

Untreated and unmodified PC, with a high content of other metals (primarily Cr, Cu, and Pb), was used in these experiments. Consequently, there was a need to investigate possible metal leaching in the dye solution after the applied Fenton process, when the pH value of the examined effluent after the treatment was ~2.5. These metals can also influence Fenton reactions. Based on the previous research of Strlič et al. [57], the presence of Cd and Zn does not lead to the significant production of oxidizing species, while Ni shows very limited catalytic activity, especially in comparison to Fe. Furthermore, Cr and Cu have higher rates of oxidizing species production compared to Fe. Nevertheless, based on the iron content, we assumed that this metal was largely responsible for chain reactions. However, the contributions of other metals should not be neglected, and PC, in this way,

represents a complex catalyst, with the reached treatment efficiency being the sum of all the individual metal contributions.

The pH value and the metal content suggested the necessity of an additional step for treatment of the effluent for removing the residual leached metals. Specifically, copper and lead were leached above the emission limit values, and chromium was almost equal to its prescribed limit value, according to national legislative "Regulation on limit values of pollutants in water and deadlines for their achievement, "Official Gazette no 67" [58].

In order to remove the metals, lime was used, and it was added to the treated effluent. The pH value was maintained in the range of 7.5–8 in order to ensure the requirements were met [58]. Simultaneously, the reached pH value was close to the range where the solubility of the hydroxides of most metals is minimized [59,60]. Table 2 shows the metal concentrations measured in the solution after the heterogeneous Fenton process at predetermined optimal reaction conditions and after the pH correction (by adding lime).

**Table 2.** Metal concentrations and pH values in the tested effluents after the Fenton process and after the pH adjustment by the addition of lime.

| Effluent | Metals | | | | | | | | pH |
|---|---|---|---|---|---|---|---|---|---|
| | As | Cd | Cr | Cu | Fe | Ni | Pb | Zn | |
| | mg/L | | | | | | | | |
| After the Fenton process | 0.052 | 0.018 | 0.482 | 1.521 | 20.15 | 0.258 | 2.228 | 1.231 | 2.47 |
| After the pH adjustment | <DL | <DL | 0.043 | 0.052 | 1.203 | 0.008 | 0.012 | 0.085 | 8 |
| A | - | - | 0.5 | 0.5 | - | 0.5 | - | 2 | - |
| B | - | 0.1 | 0.5 | 0.5 | - | 0.5 | 0.5 | 2 | 6.5–9.0 |

A—emission limit values before mixing with other wastewater at the plant; B—emission limit values at the point of discharge into surface waters; DL (detection limit)/As—DL = 1.37 µg/L; Cd—DL = 0.15 µg/L.

It can be seen that the addition of lime, after the Fenton process, contributed to reducing the metal content. The emission limit values for all metals and As were met. Further characterization was performed after pH adjustments and residue separation.

The mineralization level of generated effluent is typically determined by measuring the degree of total organic carbon (TOC) removal and the chemical oxygen demand (COD) reduction. During the Fenton process, solution decolorization is caused by the destruction of the chromophore groups of dye molecules, while the removal of the COD and TOC depends on the degree of dye mineralization. COD removal is entirely dependent on the complete dye molecule mineralization. TOC reduction is primarily assigned to highly-complex dye structure fragmentation, leading to the formation of relatively simpler organic fragments, such as carboxylic acids, aldehydes, ketones, alcohols, etc. These parameters were measured in the initial solution of the RR120, as well as in the effluent after the Fenton treatment (applied at optimal conditions). The values of the parameters examined are shown in Table 3.

**Table 3.** COD and TOC values before and after application of the heterogeneous Fenton process.

| RR120 | COD mg $O_2$/L | TOC mg C/L |
|---|---|---|
| Before Fenton process | 104 | 16.1 |
| After Fenton process | 15.9 | 6.11 |
| Removal (%) | 84.7 | 62.1 |

It can be concluded that a significant degree of COD and TOC removal was achieved. Faster decolorization and COD reduction followed by a slow TOC reduction indicated the formation of stable intermediates in the reaction medium, which contributed to the higher value of this parameter [61]. In the studies by Paul et al. [62], the removal of the COD versus TOC was also more effective, particularly in the initial stage of the treatment. In order to increase the level of efficiency in terms of mineralization, it was necessary to

extend the treatment time and the concentrations of the Fenton reagents [18], although according to Labiadh et al. [25], there was no need for complete mineralization as most of organic compounds that cause toxicity would have been converted to small biodegradable molecules when the TOC removal was 50–60%.

Respirometry tests are a widely employed method for the characterization of wastewater streams to access toxic/inhibitory effects towards a biomass. The detailed characterization of such streams is fundamental for efficient operations in wastewater treatment units. Determination of the respirometry activities of industrial pollutants towards biological activated sludge is a useful and convenient parameter for the assessment and control of acute toxicity and microbial inhibition [63–66]. In this research, respirometry measurements were conducted to investigate the comparisons of the biodegradability and toxicity of the tested effluent before and after the Fenton process was applied. The results, presented in Figure 4, indicated that there was an increase in oxygen consumption after the applied heterogeneous Fenton process. The increased oxygen consumption indicated the higher biodegradability of the compounds in the treated effluent, as well as the absence of toxic effects of the resulting oxidation intermediates towards the microorganisms that carry out biodegradation. This effect was particularly pronounced in the initial phase of the process, where for the untreated effluents, the inhibition of the microorganisms phenomena was observed.

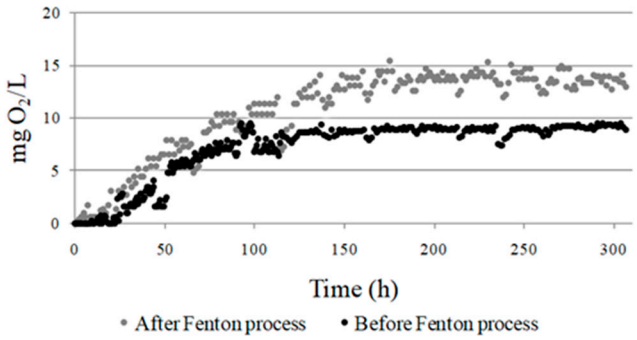


**Figure 4.** Respirometry measurements before and after the Fenton treatment.

Testing the toxicity and biodegradability is of particular importance in the case of applications of the Fenton process for the treatment of colored effluents. This treatment improves the biodegradability and reduces the toxicity of effluents containing textile dyes synthesized intentionally to be photo, chemically, and biochemically stable, as well as resistant to biodegradation. Therefore, the oxidation of the xenobiotic by the Fenton process can be considered an effective method of pre-treatment for non-biodegradable wastewater, making them amenable to conventional biological treatment [67–69].

Bioluminescence tests were performed in a mixture at the beginning of the process (time zero) when the optimal operating conditions were used (pH of 3, 10 mM of $H_2O_2$, 4 g/L of PC, and 50 mg/L of RR120), and they promoted an inhibition rate of 98% (Figure 5). After 480 min, the pH increased to a neutral level, and residue separation and inhibition decreased to 52%. Luminescence was measured again in the reaction mixture after an additional 8 h, when the detected inhibition was 45%. Very high toxicity in the beginning of a process is a reflection of a high dye concentration, the presence of hydrogen-peroxide, and possible metal leaching from PC. After 480 min, the inhibition originated from the formed dye molecule intermediates. As the reaction proceeded, there was a complete exhaustion of $H_2O_2$ and the concentration of the intermediate aromatics products decreased, resulting in the detoxification of the treated solution. Similar results have been reported in the literature [2,9,70,71].

To study the degradation of the RR120 with PC in a Fenton-like process, UV-Vis spectral changes in the aqueous solution as a function of the reaction time were recorded (Figure 6).The UV-VIS absorption spectrum of the RR120 showed two absorption peaks: one in the UV region ($\lambda_{max}$ = 290 nm) and another doublet peak in the visible region

($\lambda_{max}$ = 512–540 nm). The UV band was characteristic of the p-conjugated naphthalene ring, whereas the strong doublet absorption bands in the visible region appeared due to its conjugation through the hydrazone unit [62]. The doublet peaks at 512 and 540 nm decreased as the reaction proceeded, and they eventually disappeared, indicating that the azo link had been broken down. The peaks in the UV region (290, 245, and 210 nm) were largely attributed to naphthalene, the benzene ring, and other aromatics structures [2]. These absorption peaks also decreased in later phases of the reaction, indicating total dye molecule destruction.

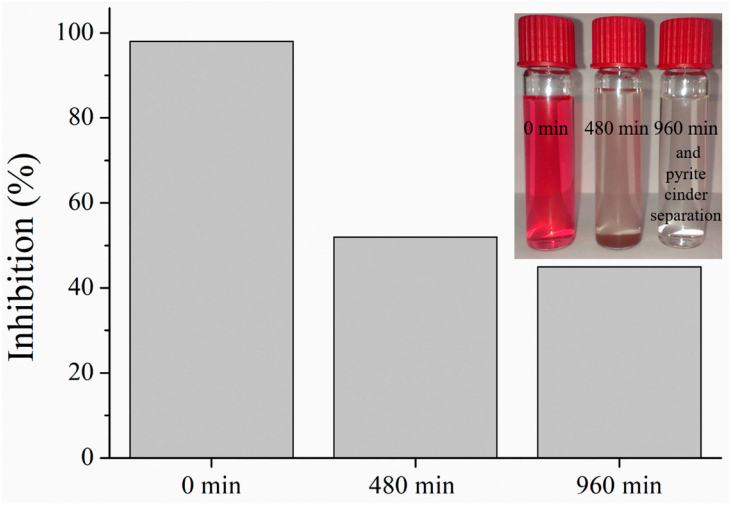


**Figure 5.** Inhibition of the RR120 before and after degradation under optimal conditions.

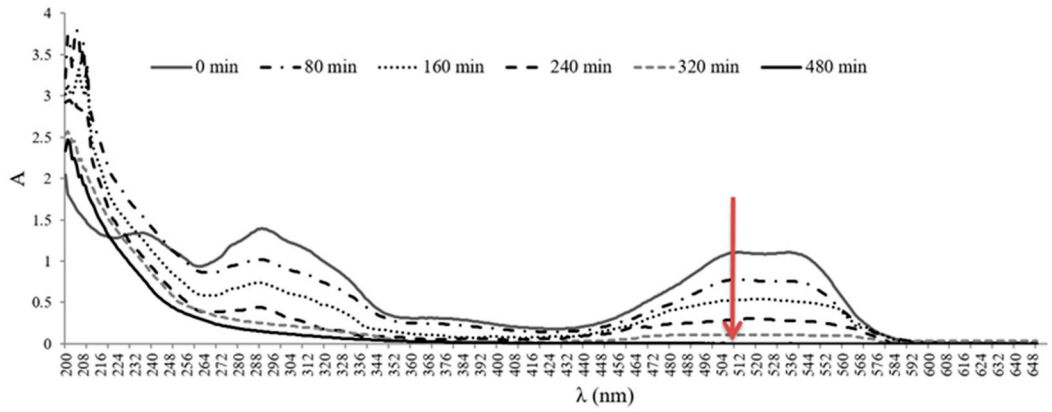


**Figure 6.** The UV-VIS spectral variations with reaction time.

Qualitative GC/MS analysis was used to identify the primary compounds and intermediates formed during the degradation process. The obtained compounds in the effluent after treatment, as well as in sample containing only PC and $H_2O_2$ in optimal dosages, were recognized as having a probability of higher than 70%, and they are presented in Table 4. The proposed degradation pathway for the RR120 by Fenton oxidation is shown in Figure 7. In general, HO• radicals may react by the abstraction of hydrogen atoms, in addition to unsaturated bonds or direct electron transfer reactions. In the case of azo dyes, HO• radicals participate in addition reactions that trigger the oxidation of either azo linkages or aromatic structures [9]. The proposed mechanism would consist of three phases: (1) oxidative transformation of the azo groups, leading to immediate visual decolorization where the azo group was converted into amino and nitroso groups, finally leading to the formation of amino benzene (D7) and N-nitrosodimethylamine (D15), and at the end, to deamination; (2) the cleavage of the C-N bonds, forming the molecule 6-chloro-n-ethyl-n'-(propan-2-yl)-1,3,5-triazine-2,4-diamine hydrochloride (D3), as well

as derivates with conjugated benzene and naphthalene rings, such as Bis(2-ethylhexyl) phthalate (D1), 1,2-Benzenedicarboxylic acid, bis (2-methylpropyl) ester (D2), Benzene sulphonic acid (D4), and Dibutyl phthalate (D5), and the obtained molecules undergo further mineralization, creating simpler products such as phthalic anhydride (D6), naphtalen-1-ol (D8), and diethyl phthalate (D9); and (3) ring opening reactions, forming intermediates such as sodium octyl sulphate (D10), decana, (D11), pentanoic acid (D12), pentanedioic acid (D13), and 2-Undecene, 5-methyl- (D14). The results confirmed that the decomposition of the dye molecules followed the direction of creating a simpler aromatic and aliphatic intermediates and products formed by "opening" the aromatic rings, leading to the end oxidation products, $CO_2$, $H_2O$, and inorganic compounds, which is in accordance with the literature data [2,16,50,72,73]. However, complete mineralization to $CO_2$ and $H_2O$ was not possible, which is in accordance with the TOC results.

**Table 4.** The GC-MS-identified primary components during RR120 degradation.

| CAS Number | Compounds | | RR120 Synthetic Solution after Treatment | PC + $H_2O_2$ + d$H_2O$ |
|---|---|---|---|---|
| 85-44-9 | Phthalic anhydride | D6 | ♦ | |
| 96-76-4 | Phenol and 2,4-bis(1,1-dimethylethyl)- | | ♦ | ♦ |
| 112-42-5 | 1-Undecanol | | ♦ | ♦ |
| 1921-70-6 | Pentadecane and 2,6,10,14-tetramethyl- | | ♦ | ♦ |
| 112-39-0 | Hexadecanoic acid and methyl ester | | ♦ | ♦ |
| 84-74-2 | Dibutyl phthalate | D5 | ♦ | |
| 117-81-7 | Bis(2-ethylhexyl) phthalate | D1 | ♦ | |
| 104-76-7 | 1-Hexanol and 2-ethyl- | | | ♦ |
| 84-66-2 | Diethyl phthalate | D9 | ♦ | |
| 544-63-8 | Tetradecanoic acid | | | ♦ |
| 62-75-9 | N-Nitrosodimethylamine | D15 | ♦ | |
| 62-53-3 | Amino benzene | D7 | ♦ | |
| 287476-17-9 | 6-chloro-n-ethyl-n′-(propan-2-yl)-1,3,5-triazine-2,4-diamine hydrochloride | D3 | ♦ | |
| 98-11-3 | Benzene sulphonic acid | D4 | ♦ | |
| 90-15-3 | Naphtalen-1-ol | D8 | ♦ | |
| 84-69-5 | 1,2-Benzenedicarboxylic acid and bis (2-methylpropyl) ester | D2 | ♦ | |
| 142-31-4 | Sodium octyl sulfate | D10 | ♦ | |
| 112-31-2 | Decanal | D11 | ♦ | |
| 109-52-4 | Pentanoic acid | D12 | ♦ | |
| 110-94-1 | Pentanedioic acid | D13 | ♦ | |
| 56851-34-4 | 2-Undecene and 5-methyl- | D14 | ♦ | |

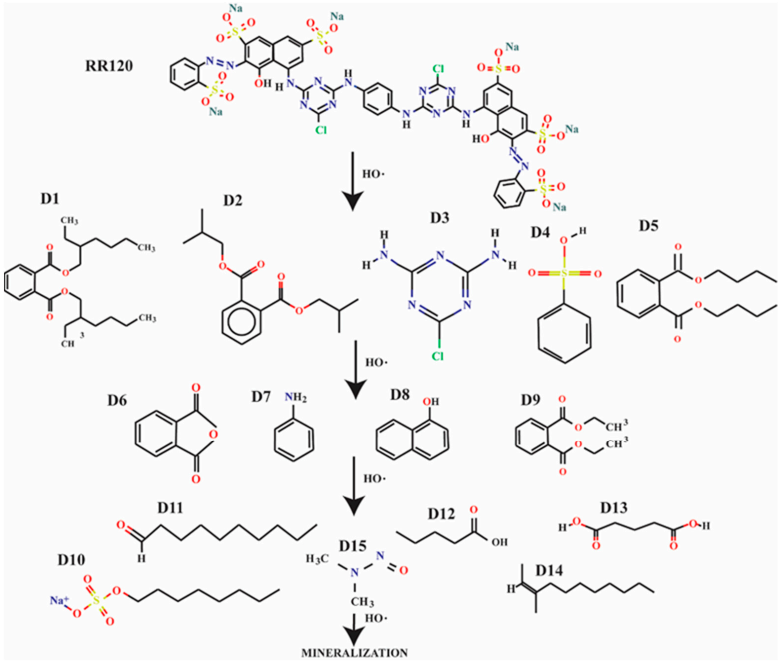


**Figure 7.** Proposed mechanism of RR120 degradation under optimal conditions.

## 3. Materials and Methods

Commercial RR120 (CAS: 61951-82-4) (Table 5), $H_2O_2$ (30wt. %), $H_2SO_4$, NaOH, and quicklime (99% CaO) were obtained from Sigma-Aldrich (Merck Group, St. Louis, USA). All the chemicals used were of analytical grade, without further purification. The PC used in this work represented a residue after the pyrite combustion process in the sulphuric production industry unit of "ICP Prahovo", Prahovo, Republic of Serbia. The PC was washed three times in deionized water prior to conducting the experiment and then dried for an hour at 105 °C.

**Table 5.** Chemical structure and characteristics of the Reactive Red 120 azo dye.

| | |
|---|---|
| Chemical structure | 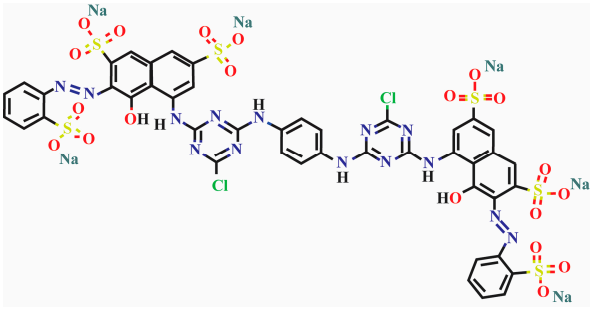 |
| Chemical name | Reactive Red 120 |
| Abbreviation | RR120 |
| Chemical formula | $C_{44}H_{24}Cl_2N_{14}O_{20}S_6Na_6$ |
| CAS | 61951-82-4 |
| Molar mass (g/mol) | 1469.98 |
| $\lambda_{max}$ (nm) | 512 |

All solutions were prepared with deionized water. The experiments were performed at room temperature (25 ± 0.5 °C).

### *3.1. PC Characterization*

A scanning electron microscope with an energy-dispersive X-ray (SEM-EDX) (SEM; Hithchi S-4700 Type II, Hitachi High-Tech Corporation, Tokyo, Japan) was used for recording images to determine the morphologies and particle size distributions. X-ray diffraction (Philips PW 1710 automated X-ray powder diffractometer, Philips Electronics, Alabama, USA) was used for the identification of the main chemical species in the PC sample. Afterwards, the chemical composition of the PC was determined by X-ray diffraction (XRD) in combination with X-ray fluorescence (XRF) spectrometry (S8 Tiger, Bruker, Bruker Corporation, Billerica, MA, USA). Structural analysis was performed using 77 K $N_2$ adsorption-desorption isotherms with an Autosorb iQ Surface Area Analyzer (Quantachrome Instruments, Anton Paar GmbH, Graz, Austria). Samples were outgassed at 120 °C for 2 h before running the isotherms. A multi-point BET (Brunauer-Emmett-Teller) method was used to determine the specific surface area. Mesopore volumes were derived from the desorption isotherms using the BJH (Barrett–Joyner-Halenda) model, and micropore volumes were calculated using the t-test method.

### *3.2. Optimization of Operating Conditions for Dye Solution Decolorization*

All experiments were performed on a jar test apparatus (FC6S Velp Scientifica, VELP Scientifica, Usmate Velate, Italy) where reactive mixtures of 0.25 L volumes were continually mixed in 1 L laboratory cups at 150 rpm. The first comparison of the RR120 decolorization efficiency in the various processes, when using only PC, $H_2O_2$, and the Fenton process, was examined in order to establish the contribution of each process.

Optimization experiments were performed according to the following procedure: firstly, the appropriate PC dosage was added to the model dye solution, and then we

proceeded with the pH adjustment to the desired value with the addition of the required amount of $H_2O_2$. After reaction, the samples were centrifuged at 4000 rpm for 12 min to remove the solid particles. The aliquots were subsequently filtered through a 0.45 µm pore size membrane filter and immediately analyzed afterward. The UV spectra and decolorization of the synthetic dye solution were monitored by absorbance (A) at $\lambda$max = 512 nm (UV/VIS spectrophotometer, SHIMADZU, Kyoto, Japan). The pH was adjusted with $H_2SO_4$ and NaOH and measured by a pH meter (inoLab pH/ION 735, WTW GmbH, Xylem Inc., Washington, DC, USA). The efficacy of the dye solution decolorization was determined by the application of the following formula (12):

$$\text{Decolorization efficiency (\%)} = ((A_0 - A_t)/A_0) * 100\%, \quad (12)$$

where $A_0$ represents the initial absorbance of the dye solution and $A_t$ represents the absorbance of the dye solution after a certain time t.

The mathematical model of the author Behnajady et al. was employed to describe the decolorization kinetic analysis [74]. This model was chosen because the whole process cannot be described by a simple reaction kinetic.

$$t/(1 - (A_t/A_0)) = m + bt \quad (13)$$

In this linearized form of equation, $A_t$ represents the absorbance value obtained after a time t (min), $A_0$ represents the initial absorbance of the dye solution at $\lambda_{max}$, and b and m are characteristic constants which indicate the reaction kinetics model and decolorization.

### *3.3. Effluent Characterization*

Characterization of the generated effluent in terms of leached metals and arsenic was performed before and after adjusting the pH to 7.5–8 by atomic absorption spectrometry (AAS) (Perkin Elmer AAnalyst ™ 700, Waltham, MA, USA) according to standard procedures [75,76]. Determination of the mineralization of the obtained effluent was performed by total organic carbon (TOC) measurements using an Elementar Liqui TOCII analyzer (Elementar Analysensysteme GmbH, Langenselbold, Germany). The obtained effluent was characterized in terms of chemical oxygen demand (COD) using the standard method in ISO 6060: 1994 [77].

Respirometry measurements were performed using the OxiTop OC110 system (WTW GmbH, Xylem Inc., Washington, DC, USA) [78], wherein the oxygen consumption was determined in the investigated effluent before and after the Fenton treatment was applied. The potential toxicity of the treated solution was examined using the inhibitory effect on the light emission of the luminescent bacteria Vibrio fischeri (LUMIStherm, LUMIStox and LUMISsoftIV software, HACH-LANGE GmbH, Düsseldorf, Germany) according to the method in ISO 11348-1:2007 [79].

A qualitative gas chromatographic/mass spectrometric (GC/MS screening) analysis was used to identify the nature of the degradation products in the treated effluent, as well as in the blank sample without a dye molecule. Samples were prepared by extraction with hexane and dichloromethane according to Jóźwiak et al. [80] and Pachhade et al. [81].

## 4. Conclusions

In this study, the decolorization and degradation extent of RR120 in a heterogeneous Fenton-like PC/$H_2O_2$ system was evaluated, and the obtained effluent was thoroughly characterized. The following conclusions can be made:

i. The PC characterization, in terms of structure, composition, and iron oxides content, indicated that this material can be considered as a promising catalyst in Fenton-like systems.
ii. PC demonstrated superior catalyst features for the decolorization of azo dye RR120 in a modified Fenton process. Under the optimal conditions (RR120 = 50 mg/L, PC = 4 g/L, $H_2O_2$ = 10 mM, and pH = 3) decolorization of 92% was achieved.

iii. The metal content in the resulting effluent suggested the necessity for an additional treatment step (the addition of lime) in order to remove the leached metals and As.
iv. A notable degree of mineralization was achieved under the applied condition (85% and 62% of COD and TOC removal, respectively).
v. The respirometry measurements showed increased oxygen consumption, indicating the higher biodegradability of the compounds in the treated effluent and the absence of the toxic effects of resulting oxidation intermediates towards the microorganisms that carry out biodegradation. The bioluminescence test showed that as the Fenton-like reactions proceeded, inhibition was reduced to 45% (originating from the simpler dye molecule intermediates).
vi. The UV-VIS and GC/MS analysis confirmed that the azo link was broken down, and the later decomposition of the dye molecules proceeded in the direction of creating simpler aromatic and aliphatic intermediates.

Furthermore, the fact that the waste material can be used in a modified Fenton process as a source of catalytic iron for dye degradation represents an economically feasible method and alternative approach for its disposal, along with the minimization of possible negative environmental effects.

**Author Contributions:** D.K.: investigation, writing—original draft, resources, project administration, and funding acquisition; M.B.-T.: visualization, writing—review and editing, and supervision; V.G.: methodology and data curation; A.K.M.: software, methodology, and data curation; A.L.M.: writing—review and editing; D.T.P.: methodology and writing—review and editing; and V.P.: conceptualization and writing—review and editing. All authors have read and agreed to the published version of the manuscript.

**Funding:** This research was funded by the Science Fund of the Republic of Serbia—Program for excellent projects of young researchers—PROMIS (WasteWaterForce Project 6066881).

**Data Availability Statement:** The datasets generated during and/or analyzed during the current study are not publicly available due to intellectual property or confidentiality concerns, but they are available from the corresponding author on reasonable request.

**Acknowledgments:** The authors would like to acknowledge the University Center for Electron Microscopy-Novi Sad/Electronic laboratory microscopy (Miloš Bokorov) for the use of the measurement equipment and for their data analysis.

**Conflicts of Interest:** The authors declare that they have no known competing financial interests or personal relationships that could have appeared to influence the work reported in this paper.

## References

1. Santos, O.D.S.H.; de Freitas Carvalho, C.; da Silva, G.A.; Dos Santos, C.G. Manganese ore tailing: Optimization of acid leaching conditions and recovery of soluble manganese. *J. Environ. Manag.* **2015**, *147*, 314–320. [CrossRef] [PubMed]
2. Zheng, J.; Gao, Z.; He, H.; Yang, S.; Sun, C. Efficient degradation of Acid Orange 7 in aqueous solution by iron ore tailing Fenton-like process. *Chemosphere* **2016**, *150*, 40–48. [CrossRef] [PubMed]
3. Ajmal, A.; Majeed, I.; Malik, R.N.; Idriss, H.; Nadeem, M.A. Principles and mechanisms of photocatalytic dye degradation on $TiO_2$ based photocatalysts: A comparative overview. *RSC Adv.* **2014**, *4*, 37003–37026. [CrossRef]
4. Bae, S.; Kim, D.; Lee, W. Degradation of diclofenac by pyrite catalyzed Fenton oxidation. *Appl. Catal. B Environ.* **2013**, *134–135*, 93–102. [CrossRef]
5. Becelic-Tomin, M.; Dalmacija, B.; Rajic, L.; Tomasevic, D.; Kerkez, D.; Watson, M.; Prica, M. Degradation of anthraquinone dye Reactive Blue 4 in pyrite ash catalyzed Fenton reaction. *Sci. World J.* **2014**, *2014*, 234654. [CrossRef] [PubMed]
6. Tiberg, C.; Bendz, D.; Theorin, G.; Kleja, D.B. Evaluating solubility of Zn, Pb, Cu and Cd in pyrite cinder using leaching tests and geochemical modelling. *Appl. Geochem.* **2017**, *85*, 106–117. [CrossRef]
7. Li, H.; Li, X.; Xiao, T.; Chen, Y.; Long, J.; Zhang, G.; Zhang, P.; Li, C.; Zhuang, L.; Li, K. Efficient removal of thallium(I) from wastewater using flower-like manganese dioxide coated magnetic pyrite cinder. *Chem. Eng. J.* **2018**, *353*, 867–877. [CrossRef]
8. Tomin, M.B.; Kulic, A.; Kerkez, D.; Prica, M.; Rapajic, S.; Pilipovic, D.T.; Pesic, V. Reactive dye degradation using Fe-loaded bentonite as a Fenton-like catalyst: From process optimization to effluent acute toxicity. *Fresen. Environ. Bull.* **2017**, *26*, 569–583.
9. Donadelli, J.A.; Carlos, L.; Arques, A.; Einschlag, F.S.G. Kinetic and mechanistic analysis of azo dyes decolorization by ZVI-assisted Fenton systems: pH dependent shift in the contributions of reductive and oxidative transformation pathways. *Appl. Catal. B Environ.* **2018**, *231*, 51–61. [CrossRef]

10. Oladipo, A.A.; Ifebajo, A.O.; Gazi, M. Magnetic LDH-based CoO–$NiFe_2O_4$ catalyst with enhanced performance and recyclability for efficient decolorization of Azo dye via Fenton-like reactions. *Appl. Catal. B Environ.* **2019**, *243*, 243–252. [CrossRef]
11. Li, F.; Xia, Q.; Gao, Y.; Cheng, Q.; Ding, L.; Yang, B.; Tian, Q.; Ma, C.; Sand, W.; Liu, Y. Anaerobic biodegradation and decolorization of a refractory acid dye by a forward osmosis membrane bioreactor. *Environ. Sci. Water Res. Technol.* **2018**, *4*, 272–280. [CrossRef]
12. Gioia, L.; Ovsejevi, K.; Manta, C.; Míguez, D.; Menéndez, P. Biodegradation of acid dyes by an immobilized laccase: An ecotoxicological approach. *Environ. Sci. Water Res. Technol.* **2018**, *4*, 2125–2135. [CrossRef]
13. Govindan, K.; Raja, M.; Maheshwari, S.U.; Noel, M. Analysis and understanding of amido black 10B dye degradation in aqueous solution by electrocoagulation with the conventional oxidants peroxomonosulfate, peroxodisulfate and hydrogen peroxide. *Environ. Sci. Water Res. Technol.* **2015**, *1*, 108–119. [CrossRef]
14. Kerkez, D.V.; Tomašević, D.D.; Kozma, G.; Bečelić-Tomin, M.R.; Prica, M.D.; Rončević, S.D.; Kukovecz, A.; Dalmacija, B.D.; Kónya, Z. Three different clay-supported nanoscale zero-valentiron materials for industrial azo dye degradation: A comparative study. *J. Taiwan Inst. Chem. Eng.* **2014**, *45*, 2451–2461. [CrossRef]
15. Dou, J.; Yin, S.; Chong, J.Y.; Zhang, B.; Han, J.; Huang, Y.; Xu, R. Carbon spheres anchored Co3O4 nanoclusters as an efficient catalyst for dye degradation. *Appl. Catal. A Gen.* **2016**, *513*, 106–115. [CrossRef]
16. Milidrag, G.P.; Prica, M.; Kerkez, D.; Dalmacija, B.; Kulic, A.; Pilipovic, D.T.; Tomin, M.B. A comparative study of the decolorization capacity of the solar-assisted Fenton process using ferrioxalate and Al, Fe bentonite catalysts in a parabolic trough reactor. *J. Taiwan Inst. Chem. Eng.* **2018**, *93*, 436–449. [CrossRef]
17. Arslan-Alaton, I.; Gursoy, B.H.; Schmidt, J.-E. Advanced oxidation of acid and reactive dyes: Effect of Fenton treatment on aerobic, anoxic and anaerobic processes. *Dye. Pigment.* **2008**, *78*, 117–130. [CrossRef]
18. Babuponnusami, B.; Muthukumar, K. A review on Fenton and improvements to the Fenton process for wastewater treatment. *J. Environ. Chem. Eng.* **2014**, *2*, 557–572. [CrossRef]
19. Shoaebargh, S.; Karimi, A.; Dehghan, G. Performance study of open channel reactor on AO7 decolorization using glucose oxidase/$TiO_2$/polyurethane under UV-VIS LED. *J. Taiwan Inst. Chem. Eng.* **2014**, *45*, 1677–1684. [CrossRef]
20. Rache, M.L.; García, A.R.; Zea, H.R.; Silva, A.M.; Madeira, L.M.; Ramírez, J.H. Azo-dye orange II degradation by the heterogeneous Fenton-like process using a zeolite Y-Fe catalyst—Kinetics with a model based on the Fermi's equation. *Appl. Catal. B Environ.* **2014**, *146*, 192–200. [CrossRef]
21. Gozmen, B.; Kayan, B.; Gizir, A.M.; Hesenov, A. Oxidative degradations of reactive blue 4 dye by different advanced oxidation methods. *J. Hazard. Mater.* **2009**, *168*, 129–136. [CrossRef] [PubMed]
22. Chang, M.-W.; Chern, J.-M. Decolorization of peach red azo dye, HF6 by Fenton reaction: Initial rate analysis. *J. Taiwan Inst. Chem. E* **2010**, *41*, 221–228. [CrossRef]
23. Ilinoiu, E.C.; Pode, R.; Manea, F.; Colar, L.A.; Jakab, A.; Orha, C.; Ratiu, C.; Lazau, C.; Sfarloaga, P. Photocatalytic activity of a nitrogen-doped $TiO_2$ modified zeolite in the degradation of Reactive Yellow 125 azo dye. *J. Taiwan Inst. Chem. E* **2013**, *44*, 270–278. [CrossRef]
24. Saravanan, R.; Gupta, V.K.; Narayanan, V.; Stephen, A. Visible light degradation of textile effluent using novel catalyst ZnO/$Mn_2O_3$. *J. Taiwan Inst. Chem. E* **2014**, *45*, 1910–1917. [CrossRef]
25. Labiadh, L.; Oturan, M.A.; Panizza, M.; Ben Hamadi, N.; Ammar, S. Complete removal of AHPS synthetic dye from water using new electro-Fenton oxidation catalyzed by natural pyrite as heterogeneous catalyst. *J. Hazard. Mater.* **2015**, *297*, 34–41. [CrossRef] [PubMed]
26. Saravanan, A.; Deivayanai, V.; Kumar, P.S.; Rangasamy, G.; Hemavathy, R.; Harshana, T.; Gayathri, N.; Alagumalai, K. A detailed review on advanced oxidation process in treatment of wastewater: Mechanism, challenges and future outlook. *Chemosphere* **2022**, *308*, 136524. [CrossRef]
27. Hu, Q.; Xu, L.; Fu, K.; Zhu, F.; Yang, T.; Yang, T.; Luo, J.; Wu, M.; Yu, D. Ultrastable MOF-based foams for versatile applications. *Nano Res.* **2022**, *15*, 2961–2970. [CrossRef]
28. Hu, Q.; Zhang, M.; Xu, L.; Wang, S.; Yang, T.; Wu, M.; Lu, W.; Li, Y.; Yu, D. Unraveling timescale-dependent Fe-MOFs crystal evolution for catalytic ozonation reactivity modulation. *J. Hazard. Mater.* **2022**, *431*, 128575. [CrossRef]
29. Guo, D.; Liu, Y.; Ji, H.; Wang, C.-C.; Chen, B.; Shen, C.; Li, F.; Wang, Y.; Lu, P.; Liu, W. Silicate-Enhanced Heterogeneous Flow-Through Electro-Fenton System Using Iron Oxides under Nanoconfinement. *Environ. Sci. Technol.* **2021**, *55*, 4045–4053. [CrossRef]
30. Loeb, S.K.; Alvarez, P.J.J.; Brame, J.A.; Cates, E.L.; Choi, W.; Crittenden, J.; Dionysiou, D.D.; Li, Q.; Li-Puma, G.; Quan, X.; et al. The Technology Horizon for Photocatalytic Water Treatment: Sunrise or Sunset? *Environ. Sci. Technol.* **2019**, *53*, 2937–2947. [CrossRef]
31. Zhang, Y.; Liu, C.; Xu, B.; Qi, F.; Chu, W. Degradation of benzotriazole by a novel Fenton-like reaction with mesoporous Cu/MnO2: Combination of adsorption and catalysis oxidation. *Appl. Catal. B Environ.* **2016**, *199*, 447–457. [CrossRef]
32. Nidheesh, P.V. Heterogeneous Fenton catalysts for the abatement of organic pollutants from aqueous solution: A review. *RSC Adv.* **2015**, *5*, 40552–40577. [CrossRef]
33. Zhang, B.; Li, X.; Akiyama, K.; Bingham, P.A.; Kubuki, S. Elucidating the Mechanistic Origin of a Spin State-Dependent FeNx−C Catalyst toward Organic Contaminant Oxidation via Peroxymonosulfate Activation. *Environ. Sci. Technol.* **2022**, *56*, 1321–1330. [CrossRef] [PubMed]

34. Yang, T.; Yu, D.; Wang, D.; Yang, T.; Li, Z.; Wu, M.; Petru, M.; Crittenden, J. Accelerating Fe(III)/Fe(II) cycle via Fe(II) substitution for enhancing Fenton-like performance of Fe-MOFs. *Appl. Catal. B Environ.* **2021**, *286*, 119859. [CrossRef]
35. Qi, C.; Wen, Y.; Zhao, Y.; Dai, Y.; Li, Y.; Xu, C.; Yang, S.; He, H. Enhanced degradation of organic contaminants by Fe(III)/peroxymonosulfate process with L-cysteine. *Chin. Chem. Lett.* **2022**, *33*, 2125–2128. [CrossRef]
36. Dai, Y.; Qi, C.; Cao, H.; Wen, Y.; Zhao, Y.; Xu, C.; Yang, S.; He, H. Enhanced degradation of sulfamethoxazole by microwave-activated peracetic acid under alkaline condition: Influencing factors and mechanism. *Sep. Purif. Technol.* **2022**, *288*, 120716. [CrossRef]
37. Peng, J.; Wang, Z.; Wang, S.; Liu, J.; Zhang, Y.; Wang, B.; Gong, Z.; Wang, M.; Dong, H.; Shi, J.; et al. Enhanced removal of methylparaben mediated by cobalt/carbon nanotubes (Co/CNTs) activated peroxymonosulfate in chloride-containing water: Reaction kinetics, mechanisms and pathways. *Chem. Eng. J.* **2021**, *409*, 128176. [CrossRef]
38. Dai, Y.; Cao, H.; Qi, C.; Zhao, Y.; Wen, Y.; Xu, C.; Zhong, Q.; Sun, D.; Zhou, S.; Yang, B.; et al. L-cysteine boosted Fe(III)-activated peracetic acid system for sulfamethoxazole degradation: Role of L-cysteine and mechanism. *Chem. Eng. J.* **2023**, *451*, 138588. [CrossRef]
39. Xue, X.; Hanna, K.; Abdelmoula, M.; Deng, N. Adsorption and oxidation of PCP on the surface of magnetite: Kinetic experiments and spectroscopic investigations. *Appl. Catal. B Environ.* **2009**, *89*, 432–444. [CrossRef]
40. Duan, H.; Liu, Y.; Yin, X.; Bai, J.; Qi, J. Degradation of nitrobenzene by Fenton-like reaction in a $H_2O_2$/schwertmannite system. *Chem. Eng. J.* **2016**, *283*, 873–879. [CrossRef]
41. Du, J.; Bao, J.; Fu, X.; Lu, C.; Kim, S.H. Mesoporous sulfur-modified iron oxide as an effective Fenton-like catalyst for degradation of bisphenol A. *Appl. Catal. B Environ.* **2016**, *184*, 132–141. [CrossRef]
42. Gao, Y.; Guo, Y.; Zhang, H. Enhanced adsorption performance for organic pollutant and its regeneration by heterogeneous visible light photo-Fenton process at circumneutral pH. *J. Hazard. Mater.* **2016**, *302*, 105–113. [CrossRef] [PubMed]
43. Khataee, A.; Gholami, P.; Sheydaei, M. Heterogeneous Fenton process by natural pyrite for removal of a textile dye from water: Effect of parameters and intermediate identification. *J. Taiwan. Inst. Chem. E* **2016**, *58*, 366–373. [CrossRef]
44. Oliveira, M.L.; Ward, C.R.; Izquierdo, M.; Sampaio, C.H.; de Brum, I.A.; Kautzmann, R.M.; Sabedot, S.; Querol, X.; Silva, L.F. Chemical composition and minerals in pyrite ash of an abandoned sulphuric acid production plant. *Sci. Total Environ.* **2012**, *430*, 34–47. [CrossRef] [PubMed]
45. Garrido-Ramírez, E.G.; Marco, J.F.; Escalona, N.; Ureta-Zañartu, M.S. Preparation and characterization of bimetallic Fe-Cuallophanenanoclays and their activity in the phenol oxidation by heterogeneous electro-Fenton reaction. *Microporous Mesoporous Mater.* **2016**, *225*, 303–311. [CrossRef]
46. Che, H.; Bae, S.; Lee, W. Degradation of trichloroethylene by Fenton reaction in pyrite suspension. *J. Hazard. Mater.* **2011**, *185*, 1355–1361. [CrossRef]
47. Daud, N.; Hameed, B.H. Decolorization of Acid Red 1 by Fenton-like process using rice husk ash-based catalyst. *J. Hazard. Mater.* **2010**, *176*, 938–944. [CrossRef]
48. Wu, D.; Feng, Y.; Ma, L. Oxidation of azo dyes by $H_2O_2$ in presence of natural pyrite. *Water Air Soil Poll.* **2013**, *224*, 1407. [CrossRef]
49. Sun, Y.; Yang, Z.; Tian, P.; Sheng, Y.; Xu, J.; Han, Y.-F. Oxidative degradation of nitrobenzene by a Fenton-like reaction with Fe-Cu bimetallic catalysts. *Appl. Catal. B Environ.* **2019**, *244*, 1–10. [CrossRef]
50. Hassan, H.; Hameed, B. Fe-clay as effective heterogeneous Fenton catalyst for the decolorization of Reactive Blue 4. *Chem. Eng. J.* **2011**, *171*, 912–918. [CrossRef]
51. Pichat, P. *Photocatalytic Degradation of Pollutants in Water and Air: Basic Concepts and Application*; Tarr, M.A., Ed.; Marcel Dekker, Inc.: New York, NY, USA, 2003; pp. 165–200.
52. Zhao, Y.; Hu, J. Photo-Fenton degradation of 17β-estradiol in presence of α-FeOOHR and $H_2O_2$. *Appl. Catal. B Environ.* **2008**, *78*, 250–258.
53. Arslan-Alaton, I.; Teksoy, S. Acid dyebath effluent pretreatment using Fenton's reagent: Process optimization, reaction kinetics and effects on acute toxicity. *Dye. Pigment.* **2007**, *73*, 31–39. [CrossRef]
54. Chen, A.; Ma, X.; Sun, H. Decolorization of KN-R catalyzed by Fe-containing Y and ZSM-5 zeolites. *J. Hazard. Mater.* **2008**, *156*, 568–575. [CrossRef] [PubMed]
55. Garcia, J.C.; Oliveira, J.L.; Silva, A.E.C.; Oliveira, C.C.; Nozaki, J.; de Souza, N.E. Comparative study of the degradation of real textile effluents by photocatalytic reactions involving UV/$TiO_2$/$H_2O_2$ and UV/$Fe^{2+}$/$H_2O_2$ systems. *J. Hazard. Mater.* **2007**, *147*, 105–110. [CrossRef]
56. Galeano, L.A.; Vicente, M.; Gil, A. Treatment of municipal leachate of landfill by Fenton-like heterogeneous catalytic wet peroxide oxidation using an Al/Fe-pillared montmorillonite as active catalyst. *Chem. Eng. J.* **2011**, *178*, 146–153. [CrossRef]
57. Strlič, M.; Kolar, J.; Šelih, V.S.; Kočar, D.; Pihlar, B. A comparative study of several transition metals in Fenton-like reaction systems at circum-neutral pH. *Acta Chim. Slov.* **2003**, *50*, 619–632.
58. Ministry of Energy, Development and Environmental Protection of Republic of Serbia. Regulation on limit values of pollutants in water and deadlines for their achievement. *Off. Gaz.* **2011**, *67*, 13–41.
59. Levasseur, B.; Blais, J.-F.; Mercier, G. Study of the metal precipitation from decontamination leachates of municipal wastes fly ash incinerators. *Environ. Technol.* **2005**, *26*, 421–431. [CrossRef]

60. SMirbagheri, S.; Hosseini, S. Pilot plant investigation on petrochemical wastewater treatmentfor the removal of copper and chromium with the objective of reuse. *Desalination* **2005**, *171*, 85–93. [CrossRef]
61. Kusvuran, E.; Gulnaz, O.; Irmak, S.; Atanur, O.M.; Yavuz, H.I.; Erbatur, O. Comparison of several advanced oxidation processes for the decolorization of Reactive Red 120 azo dye in aqueous solution. *J. Hazard. Mater.* **2004**, *109*, 85–93. [CrossRef]
62. Paul, J.; Rawat, K.; Sarma, K.; Sabharwal, S. Decoloration and degradation of Reactive Red-120 dye by electron beam irradiation in aqueous solution. *Appl. Radiat. Isot.* **2011**, *69*, 982–987. [CrossRef] [PubMed]
63. Mainardis, M.; Buttazzoni, M.; Cottes, M.; Moretti, A.; Goi, D. Respirometry tests in wastewater treatment: Why and how? A critical review. *Sci. Total Environ.* **2021**, *793*, 148607. [CrossRef] [PubMed]
64. Du, Y.; Chen, Y.; Zou, L.; Deng, S.; Li, G.; Zhang, D. Monitoring the Activated Sludge Activities Affected by Industrial Toxins via an Early-Warning System Based on the Relative Oxygen Uptake Rate (ROUR) Index. *Appl. Sci.* **2019**, *9*, 154. [CrossRef]
65. Foladori, P.; Bruni, L.; Tamburini, S. Toxicant inhibition in activated sludge: Fractionation of the physiological status of bacteria. *J. Hazard. Mater.* **2014**, *280*, 758–766. [CrossRef] [PubMed]
66. Santos-Juanes, L.; Amat, A.; Arques, A.; Bernabeu, A.; Silvestre, M.; Vicente, R.; Añó, E. Activated sludge respirometry to assess solar detoxification of a metal finishing effluent. *J. Hazard. Mater.* **2008**, *153*, 905–910. [CrossRef]
67. Dalzell, D.J.B.; Alte, S.; Aspichueta, E.; de la Sota, A.; Etxebarria, J.; Gutierrez, M.; Hoffmann, C.; Sales, D.; Obst, U.; Christofi, N. A comparison of five rapid direct toxicity assessment methods to determine toxicity of pollutants to activated sludge. *Chemosphere* **2002**, *47*, 535–545. [CrossRef]
68. Tekin, H.; Bilkay, O.; Ataberk, S.S.; Balta, T.H.; Ceribasi, I.H.; Sanin, F.D.; Dilek, F.B.; Yetis, U. Use of Fenton oxidation to improve the biodegradability of a pharmaceutical wastewater. *J. Hazard. Mater.* **2006**, *136*, 258–265. [CrossRef]
69. Farre, M.J.; Franch, M.I.; Ayllon, J.A.; Peral, J.; Domènech, X. Biodegradability of treated aqueous solutions of biorecalcitrant pesticides by means of photocatalytic ozonation. *Desalination* **2007**, *211*, 22–33. [CrossRef]
70. Zhang, F.; Yediler, A.; Liang, X. Decomposition pathways and reaction intermediate formation of the purified, hydrolyzed azo reactive dye C.I. Reactive Red 120 during ozonation. *Chemosphere* **2007**, *67*, 712–717. [CrossRef]
71. Dias, F.F.; Oliveira, A.A.; Arcanjo, A.P.; Moura, F.C.; Pacheco, J.G. Residue-based iron catalyst for the degradation of textile dye via heterogeneous photo-Fenton. *Appl. Catal. B Environ.* **2016**, *186*, 136–142. [CrossRef]
72. Xu, L.; Zhao, H.; Shi, S.; Zhang, G.; Ni, J. Electrolytic treatment of C.I. Acid Orange 7 in aqueous solution using a three-dimensional electrode reactor. *Dye. Pigment.* **2008**, *77*, 158–164. [CrossRef]
73. Kecić, V.; Kerkez, Đ.; Prica, M.; Lužanin, O.; Bečelić-Tomin, M.; Tomašević Pilipović, D.; Dalmacija, B. Optimization of azo printing dye removal with oak leaves-nZVI/$H_2O_2$ system using statistically designed experiment. *J. Clean. Prod.* **2018**, *202*, 65–80. [CrossRef]
74. Behnajady, M.; Modirshahla, N.; Ghanbary, F. A kinetic model for the decolorization of C.I. Acid Yellow 23 by Fenton process. *J. Hazard. Mater.* **2007**, *148*, 98–102. [CrossRef] [PubMed]
75. *USEPA Method 7000B. Flame Atomic Absorption Spectrophotometry*; Revision 2 (February 2007), Part of Test Methods for Evaluating Solid Waste, Physical/Chemical, Hazardous Waste Test Methods/SW-846; United States Environmental Protection Agency: Washington, DC, USA, 2007.
76. *USEPA Method 7010. Graphite Furnace Absorption Spectrophotometry*; Revision 0; United States Environmental Protection Agency: Washington, DC, USA, 2007.
77. *SRPS ISO 6060: 1994*; Chemical Oxigen Demand Determination. Institute for Standardization of Serbia: Beograd, Serbia, 1994.
78. *System OxiTop® Control, OxiTop® OC110-OxiTop®-C*; BA31116de03; Wissenschaftlich-TechnischeWerkstätten GmbH: Weilheim, Germany, 2006.
79. *ISO 11348-1: 2008*; Water Quality—Determination of the Inhibitory Effect of Water Samples on the Light Emission of Vibrio fischeri (Luminiscent Bacteria Test). British Standards Institution: London, UK, 2008.
80. Jóźwiak, W.K.; Mitros, M.; Kałużna-Czaplińska, J.; Tosik, R. Oxidative decomposition of Acid Brown 159 dye in aqueous solution by $H_2O_2/Fe^{2+}$ and ozone with GC/MS analysis. *Dye. Pigment.* **2007**, *74*, 9–16. [CrossRef]
81. Pachhade, K.; Sandhya, S.; Swaminathan, K. Ozonation of reactive dye, Procion red MX-5B catalyzed by metal ions. *J. Hazard. Mater.* **2009**, *167*, 313–318. [CrossRef] [PubMed]